Electrochimica Acta 56 (2010) 913–918

Contents lists available at ScienceDirect

Electrochimica Acta

journal homepage: www.elsevier.com/locate/electacta

Effect of nickel content on the electrochemical behavior of Cu–Al–Ni alloys in chloride free neutral solutions

W.A. Badawy[a,*], M.M. El-Rabiee[b], N.H. Helal[b], H. Nady[b]

[a] Chemistry Department, Faculty of Science, Cairo University, 12 613 Giza,Egypt
[b] Chemistry Department, Faculty of Science, Fayoum University, Fayoum,Egypt

ARTICLE INFO

Article history:
Received 15 August 2010
Received in revised form
27 September 2010
Accepted 28 September 2010
Available online 21 October 2010

Keywords:
Alloys
Cu–Al–Ni
Corrosion
Impedance
Polarization

ABSTRACT

The electrochemical behavior of Cu–Al–Ni alloys in chloride free neutral solutions was investigated. The effect of Ni content on the corrosion resistance of the alloys was examined and evaluated. Conventional electrochemical techniques and electrochemical impedance spectroscopy, EIS, have been used. Potentiodynamic measurements revealed that the increase in the Ni content decreases the stability of the Cu–Al–Ni alloys. The polarization measurements were confirmed by EIS experiments. The morphology of the alloy surface was investigated by scanning electron microscopy, SEM, and surface analysis was made by energy dispersive X-ray technique. The experimental impedance data were fitted to theoretical data according to a proposed equivalent circuit model representing the electrode/electrolyte interface. The results of these experiments are discussed in reference to the potential–pH (Pourbaix) diagrams of the alloying elements.

1. Introduction

Pure copper is not stable in oxygen-containing electrolytes, especially those containing chloride ions, therefore it cannot be used in marine water applications [1]. However, in these media copper–nickel alloys with copper as the main component are largely employed when high mechanical strength, good thermal conductivity and good corrosion resistance are required [2–4]. The corrosion resistance of Cu–Ni alloys is attributed to a protective layer consisting mainly of a thin, strongly adherent inner barrier Cu_2O layer, which is in contact with the electrolyte through a porous and thick outer Cu (II) hydroxide/oxide layer [5,6]. Nickel segregates into the Cu_2O barrier layer via solid-state reaction, modifies its structure and decreases the corrosion rate of alloys [6–9]. The presence of aluminum increases the corrosion resistance of the alloy, especially in sea water, sulfuric acid and salt solutions. It provides good wear properties and resistance to high temperature oxidation [10]. The good corrosion resistance of the Cu–Al–Ni alloys is due to the formation of a protective layer of alumina, which builds up quickly on the surface post-exposure to the corrosive environment [11]. The passivation of the alloy is based on the fact that aluminum has a greater affinity towards oxygen than copper and considerable stability of Al_2O_3 than Cu_2O [11]. The corrosion behavior of Cu–Ni alloys with different Ni contents, namely, 5, 10, 30 and 65 mass% Ni, in a stagnant 0.6 mol dm^{-3} NaCl solution of pH 7.0 was studied [12]. It was found that the increase in the nickel content up to 30% decreases the corrosion resistance of the alloy. When the Ni content was ≥30% the corrosion rate decreases. The investigation of the behavior of these alloys in chloride free solutions was sporadic and did not give a fundamental understanding of the role of Ni in the corrosion and passivation behavior of the alloys.

The aim of this paper is to investigate the effect of systematic increase of the Ni content on the electrochemical behavior and stability of the Cu–Al–Ni alloys in chloride free neutral solutions. These fundamental investigations are aiming at the clarification of the mechanism of the corrosion and passivation processes taking place at the electrode/solution interface.

2. Experimental details

The working electrodes were made from commercial grade Cu–Al–Ni rods, mounted into glass tubes by two-component epoxy resin leaving an area of 0.2 cm^2 to contact the solution. The mass spectrometric analysis of the materials used in this work is presented in Table 1. The electrochemical cell was a three-electrode all-glass cell, with a platinum counter electrode and saturated calomel, SCE, reference electrode. Before each experiment, the working electrode was polished mechanically using successive grades emery papers down to 2000 grit. The elec-

* Corresponding author. Tel.: +20 2 3567 6558; fax: +20 2 35685799.
E-mail addresses: wbadawy50@hotmail.com, wbadawy@cu.edu.eg (W.A. Badawy).

0013-4686/$ – see front matter © 2010 Elsevier Ltd. All rights reserved.
doi:10.1016/j.electacta.2010.09.080

Table 1
Mass spectrometric analysis for the different electrode materials in mass%.

Sample	Cu	Al	Ni	Zn	Mn	Sn	Fe	Si	Mg	Ti
Cu–Al–5Ni	81.16	11.15	4.98	0.110	0.017	0.14	2.22	0.210	0.008	0.005
Cu–Al–10Ni	76.0	11.28	9.98	0.096	0.017	0.11	2.26	0.240	0.009	0.008
Cu–Al–30Ni	60.02	9.32	29.017	0.083	0.013	0.11	1.11	0.158	0.008	0.008
Cu–Al–45Ni	43.3	9.56	46.01	0.001	0.001	0.04	0.72	0.354	–	0.014

trode was washed thoroughly with triply distilled water, and transferred quickly to the cell. The electrochemical measurements were carried out in aqueous solutions, where analytical grade reagents and triply distilled water were always used. The test electrolytes were chloride free buffer solutions of pH 7 (113.6 mL 0.1 M KH_2PO_4 + 56.8 mL 0.1 M NaOH + 79.6 mL H_2O). The polarization experiments and electrochemical impedance spectroscopic investigations, EIS, were performed using a Voltalab PGZ 100 "All-in-one" potentiostate/galvanostate system. The potentials were referred to the standard saturated calomel electrode, SCE, (0.245 V vs. nhe). All potentiodynamic polarization experiments were carried out using a scan rate of 5 mV s^{-1}. All cyclic voltammetry measurements were carried out using a scan rate of 10 mV s^{-1}. The impedance, Z, and phase shift, θ, were recorded in the frequency domain 0.1–10^5 Hz. The superimposed ac-signal was 10 mV peak to peak amplitude. To achieve reproducibility, each experiment was carried out at least twice. Details of experimental procedures are as described elsewhere [13–15].

3. Results and discussion

3.1. Open-circuit potential measurements

The open-circuit potential (OCP) of the materials under investigation was traced over 180 min immersion in chloride free naturally aerated aqueous solution of pH 7. The results of these experiments are presented in Fig. 1. The OCP of the alloys shifts towards negative values during the period of the measurement and the steady state corrosion potential is achieved within 30 min from electrode immersion in the solution. The steady state potential of Cu–Al–45Ni showed the most negative shift compared to the other alloys (cf. Fig. 1).

3.2. Potentiodynamic measurements

The cyclic voltammograms for Cu–Al–Ni alloys containing different Ni contents were recorded and presented in Fig. 2. The scan was started at −0.8 V where a transition region, before active metal dissolution occurs, in which the current density stabilizes with potential. After commencing the potential scan at−0.8 V, low cathodic current is recorded, probably due to the formation of adsorbed species on the electrode surface such as Cu $(H_2O)_{ads}$ and/or Cu $(OH)^-_{ads}$ [16]:

$$Cu + H_2O = Cu(H_2O)_{ads} \quad (1)$$

$$Cu + OH^- = Cu(OH)^-_{ads} \quad (2)$$

The adsorption of anions on the anodized metal surface promotes dissolution or passivation with increasing potential. The metal acquires a passive behavior due to the formation of an adsorbed layer and the adsorbed species represent an intermediate state for the active dissolution [17,18]. In the anodic active region, copper goes into the solution as Cu^+ ions and the current density is continuously increased with potential [17,19]. The increase in the anodic current can be attributed to the dissolution of an adsorbed layer via Cu^+ ion formation. The anodic peak can be attributed to a dissolution/passivation process that occurs in the following way:

(a) Dissolution, which is the dissolution of the adsorbed layer according to:

$$Cu(H_2O)_{ads} + OH^- = Cu(OH)^-_{2(aq)} + H^+ + e^- \quad (3)$$

$$Cu(OH)^-_{ads} + OH^- = Cu(OH)^-_{2(aq)} + e^- \quad (4)$$

(b) Passivation i.e. the formation of a passive film of Cu_2O according to [20]:

$$2Cu(OH)^-_{2(aq)} = Cu_2O + H_2O + 2OH^- \quad (5)$$

$$2Cu(OH)^-_{ads} = Cu_2O + H_2O + 2e^- \quad (6)$$

The anodic peak can be attributed to the conversion of the outer layer of the oxide film, Cu_2O, at the oxide/solution interface to Cu(I)/Cu(II) oxide or a hydroxide according to:

$$Cu_2O + H_2O = 2CuO + 2H^+ + 2e^- \quad (7)$$

$$Cu_2O + 3H_2O = 2Cu(OH)_2 + 2H^+ + 2e^- \quad (8)$$

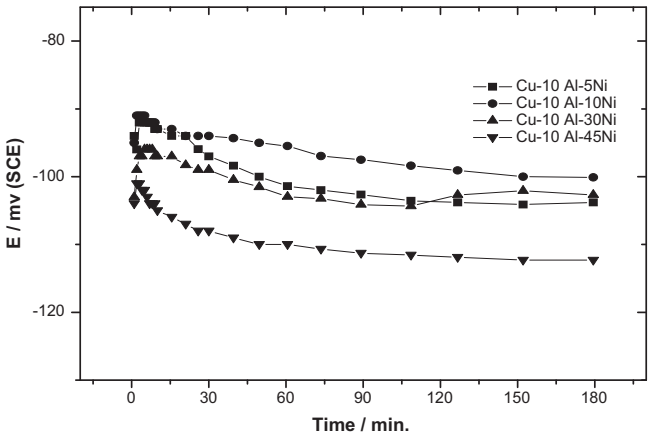

Fig. 1. Variation of the open-circuit potentials of the different Cu–Al–Ni alloys with time in chloride free naturally aerated aqueous solutions of pH 7.0 at 25 °C.

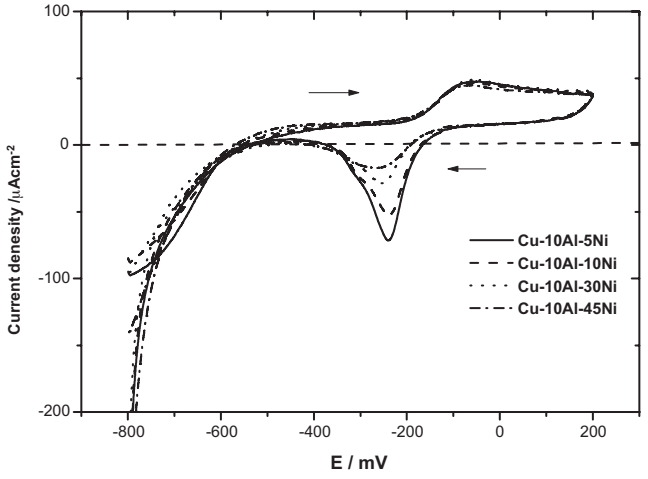

Fig. 2. Cyclic voltammograms of the different Cu–Al–Ni alloys with time in chloride free naturally aerated aqueous solutions of pH 7.0 at 25 °C and scan rate of 10 mV s^{-1}.

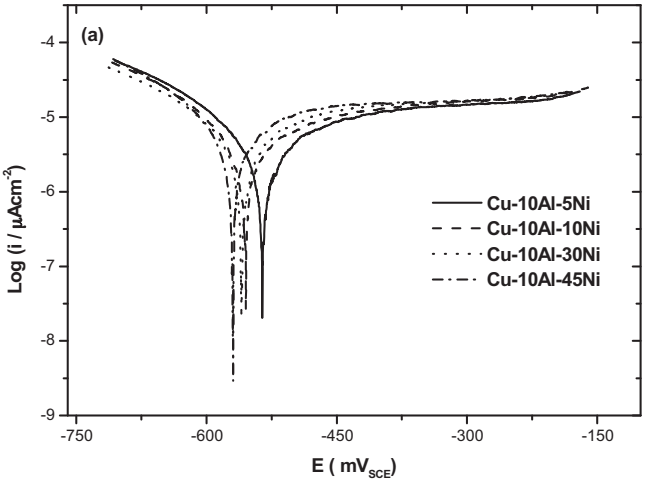

Fig. 3. Potentiodynamic polarization curves of the different Cu–Al–Ni alloys in chloride free naturally aerated aqueous solutions of pH 7.0 at 25 °C and scan rate of 5 mV s^{-1}.

The formation of the Cu_2O layer explains the decrease of the anodic current density, which can be observed as a clear peak. Also the Ni content did not affect the number and the position of anodic peak. This means that the kinetic process is controlled by the copper dissolution.

3.3. Effect of Ni content on the corrosion rate

The potentiodynamic polarization curves Cu–Al–Ni alloys with different Ni content are presented in Fig. 3. The corrosion current density, i_{corr}, and corrosion potential, E_{corr}, were calculated using potentiodynamic polarization data and presented in Table 2. The corrosion current density measured after 1 h of electrode immersion in the solution increases with increasing the Ni content. At the same time the corrosion potential was shifted to more negative values. The cathodic branch of the potentiodynamic curves represents the oxygen reduction, while the anodic one shows copper dissolution [21]. In aqueous solutions, the formation of Cu^+ takes place during the simultaneous dissolution of the alloy and the formed Cu^+ ion undergoes further oxidation to the more stable Cu^{2+} ion according to [22]:

$$Cu \rightarrow Cu^+ + e^- \quad (9)$$

$$Cu^+ \rightarrow Cu^{2+} + e^- \quad (10)$$

Then the dissolution reaction of the Cu–Al–Ni alloys can be represented by [23]:

$$(Cu + Al + Ni) + 1/2(a+b+c)O_2 + 2(a+b+c)H^+ \rightarrow aCu^{2+} + bAl^{3+} + cNi^{2+} + (a+b+c)H_2O \quad (11)$$

Table 2
Polarization parameters and rates of corrosion of the different Cu–Al–Ni alloys in chloride free naturally aerated neutral solutions, at 25 °C.

Alloys	E_{corr}/ mV	i_{corr}/μA cm^{-2}	β_a/mV	β_c/mV	Corr. rate/μm Y^{-1}
Cu–Al 5 Ni	−535	2.1	126	−80	24
Cu–Al –10Ni	−554	2.2	126	−73	25
Cu–Al –30Ni	−559	2.9	140	−94	33
Cu–Al –45Ni	−569	3.5	95	−87	38

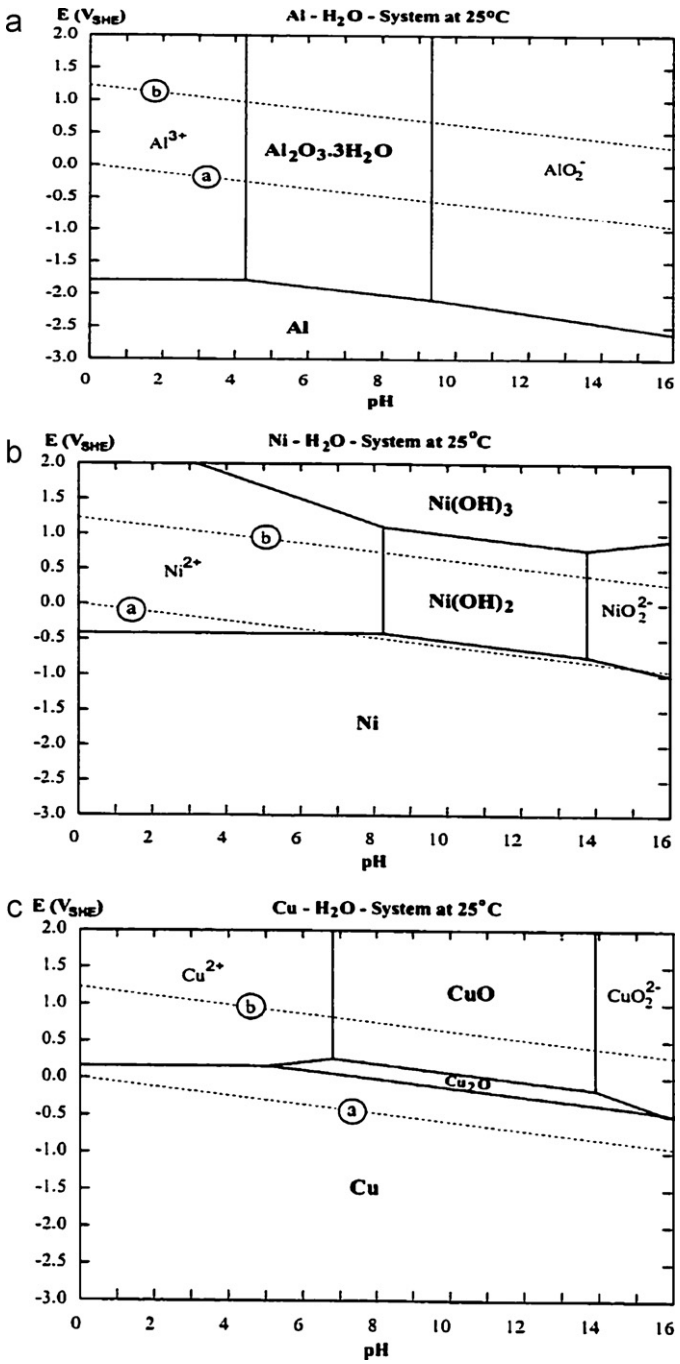

Fig. 4. Potential–pH diagrams of Cu (a), Al (b) and Ni (c) in neutral aqueous solutions.

The cathodic counter part of this overall reaction is oxygen reduction which occurs in neutral solutions according to:

$$1/2(a+b+c)O_2 + (a+b+c)H_2O + 2(a+b+c)e^- \rightarrow (a+b+c)OH^- \quad (12)$$

Generally, the corrosion behavior of the Cu–Al–Ni alloys is based on the common system of oxidation resistant materials, where Al has greater affinity towards oxygen than Cu. Under standard conditions, Al_2O_3 is almost eleven times more stable than Cu_2O relative to their metals in the zero oxidation state. For Cu–10% Al alloys, thermal oxidation is based on a rapid initial production of Cu_2O from which Al_2O_3 is achieved at the alloy/oxide interface due to

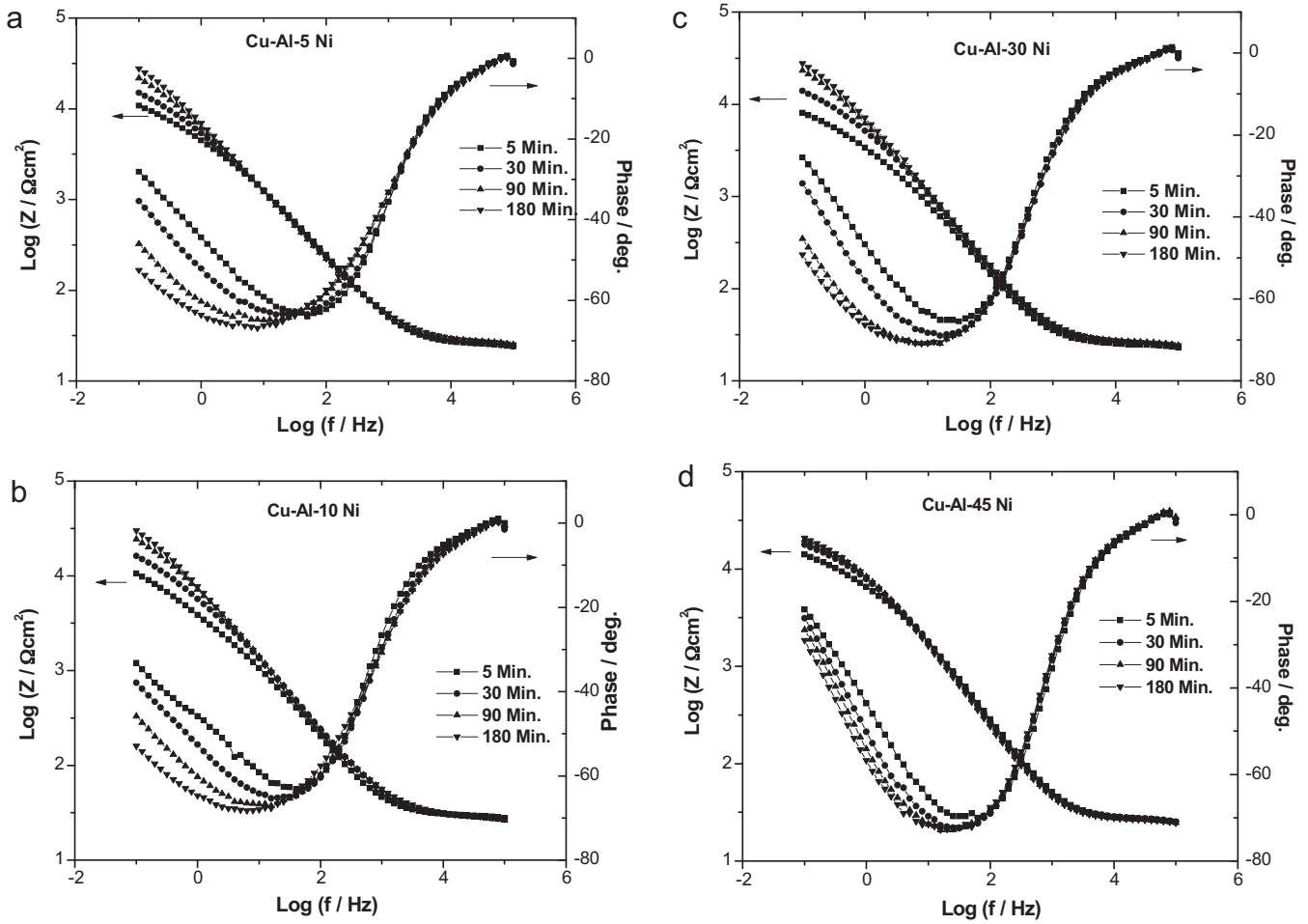

Fig. 5. Bode plots of the Cu–Al–Ni alloys after different immersion times in chloride free naturally aerated solutions of pH 7 at 25 °C. (a) 5% Ni, (b) 10% Ni, (c) 30% Ni and (d) 45% Ni.

the depletion of Cu [24]. Alumina subsequently forms as a protective oxide which is highly impermeable to the passage of cuprous cations which can no longer enter the outermost layer of cuprous oxide. The higher the aluminum content of the alloy, therefore, the greater the corrosion resistance due to the protective Al_2O_3 film since the limiting mole fraction is achieved over a shorter exposure time and is maintained at lower copper dissolution rates[24]. Keeping the Al% constant and changing the ratio of Ni the behavior becomes different because of the enrichment of Ni to the metallic surface.

The potential/pH diagrams, i.e. Pourbaix diagrams, provide a thermodynamic basis for a better understanding of metal dissolution and oxide formation phenomena in aqueous solutions at various electrochemical conditions. Regions of stability of solid and soluble species are defined at different activities based on the data of standard free energies [25]. Fig. 4(a–c) shows *E*/pH diagrams for the elements of interest (Cu, Ni and Al) in water at 25 °C. The thermodynamics data used for constructing Fig. 4 were obtained from the data base compiled by Roine [26]. Inspection of the Pourbaix diagrams for Cu, Al and Ni presented in Fig. 4 (a–c), respectively, it is clear that while Cu and Al form the most stable species, Ni is active. This explains why the increase of the Ni content, increases the corrosion rate of the alloys. It seems that incorporation of Ni consumes almost all mobile cation vacancies in the Cu_2O barrier layer decreasing its ionic and electronic conductivity [27,28]. The increase in the Ni content shows a slight shift in the E_{corr} towards more negative values. The increase in the i_{corr} can be interpreted by the dissolution of Ni with the formation of Ni^{2+}.

3.4. The electrochemical impedance measurements of Cu–Al–Ni alloys

Electrochemical impedance spectroscopy, EIS, is a powerful, non-destructive electrochemical technique for characterizing electrochemical reactions at the metal/electrolyte interface and the formation of corrosion products. The impedance spectra are recorded at the open circuit potential after different immersion times to monitor the oxide film formation on the alloys surface in chloride free naturally aerated neutral solutions. Fig. 5(a–d) shows the impedance spectra for the different Cu–Al–Ni alloys at different time intervals of electrode immersion in the solution. For all alloys, the total impedance, *Z*, increases with the exposure time, which suggests a progressive passive film formation until a steady state is achieved [29]. The increase of impedance indicates the growth of a protective oxide film on the metallic surface [13,19,22,27]. The phase maximum at low frequency is attributed to the formation of a protective layer of duplex nature [9,28]. The recorded gradual increase of the phase maximum with the increase of the immersion time indicates a decrease in the corrosion rate [27,29]. This can be clearly seen on the Nyquist format; the diameters of the semicircles of the plot increase with the increase of the time of exposure indicating an increase in the oxide film resistance (cf. Fig. 6). The impedance data were analyzed using software provided with the impedance system where the dispersion formula was used. For a simple equivalent circuit model consisting of a parallel combination of a capacitor, C_{dl}, and a resistor, R_{ct}, in series with a resistor, R_s, representing the solution resistance, the electrode impedance,

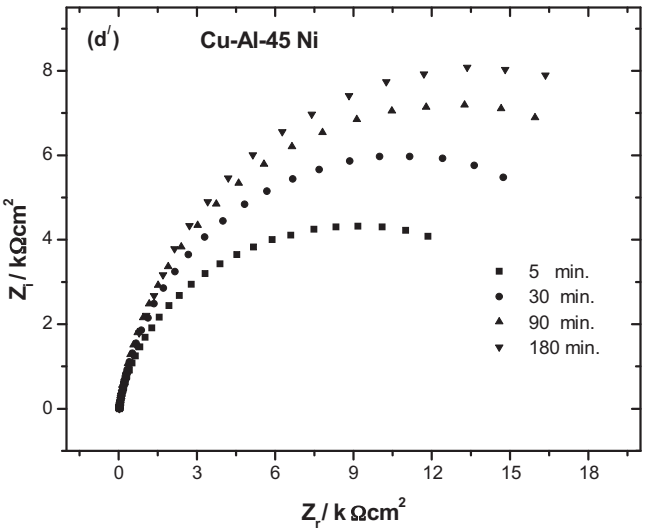

Fig. 6. Nyquist impedance plots of the Cu–10Al–45Ni alloy in chloride free naturally aerated aqueous solutions of pH 7.0 at 25 °C.

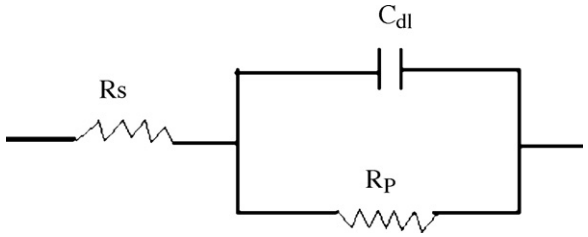

Fig. 7. Equivalent circuit model for the impedance data fitting of the Cu–Al–Ni alloys, R_s = electrolyte resistance, R_{ct} = charge transfer (corrosion) resistance, and C_{dl} = electrode capacitance.

Z, is represented by the mathematical formulation:

$$Z = \frac{Rs + Rct}{1} + (2\pi f R_{ct} C_{dl})^{\alpha} \quad (13)$$

where α denotes an empirical parameter $(0 > \alpha > 1)$ and f is the frequency in Hz. The dispersion formula takes into account the deviation from the ideal capacitor, *RC*, behavior in terms of a distribution of time constants due to surface inhomogeneties, roughness effects, and variations in properties or compositions of surface layers [30,31]. The impedance data were analyzed using the equivalent circuit model presented in Fig. 7, and the calculated equivalent circuit parameters for two of the investigated alloys representing the lower nickel content i.e. Cu–Al–5Ni and the higher nickel content i.e. Cu–Al–45Ni at different intervals of electrode immersion in the chloride free neutral solution are presented in Table 3 a and b, respectively. The presented values show the gradual increase of the corrosion resistance with the increase of the immersion time. In all cases, the value of α is nearly 1, which suggests that the barrier layer behaves like an ideal RC.

The impedance data of the different Cu–Al–Ni alloys recorded after 1 h of the alloy immersion in the chloride free neutral solutions are presented in Fig. 8a. The recorded decrease in the impedance values with increasing the Ni content is presented in Fig. 8b. The calculated equivalent circuit parameters for these measurements are presented in Table 4. The obtained impedance data for the different alloys is in good agreement with the DC measurements.

The corrosion resistance of the Cu–Al–Ni alloys is attributed to a spontaneously formed protective layer consisting mainly of a thin, inner barrier Cu_2O layer, which is in a contact with the electrolyte through a thick porous outer layer of Cu(II) hydroxide/oxide [9,12].

Table 3
Equivalent circuit parameters for two Cu–Al–Ni alloys, in chloride free naturally aerated neutral solutions, at 25 °C.

Time/min.	R_s/Ω	$R_p/k\Omega\,cm^2$	$C_{dl}/\mu F\,cm^{-2}$	α
(a) Cu–Al– 5Ni				
5	5.1	12.6	39.9	0.99
15	5.2	17.3	36.7	0.99
30	6.2	22.7	35.0	1.00
60	5.3	36.0	35.4	0.99
90	8.1	51.3	31.0	0.99
120	10.0	60.3	26.4	1.0
180	11.3	87.8	18.1	1.0
(b) Cu–Al– 45Ni				
5	6.9	12.7	25.1	0.99
15	6.2	15.6	25.5	0.99
30	4.2	18.2	27.7	0.99
60	8.5	20.9	24.1	0.99
90	4.3	21.4	29.8	0.99
120	10.1	24.7	20.4	0.99
180	2.2	23.8	33.5	0.99

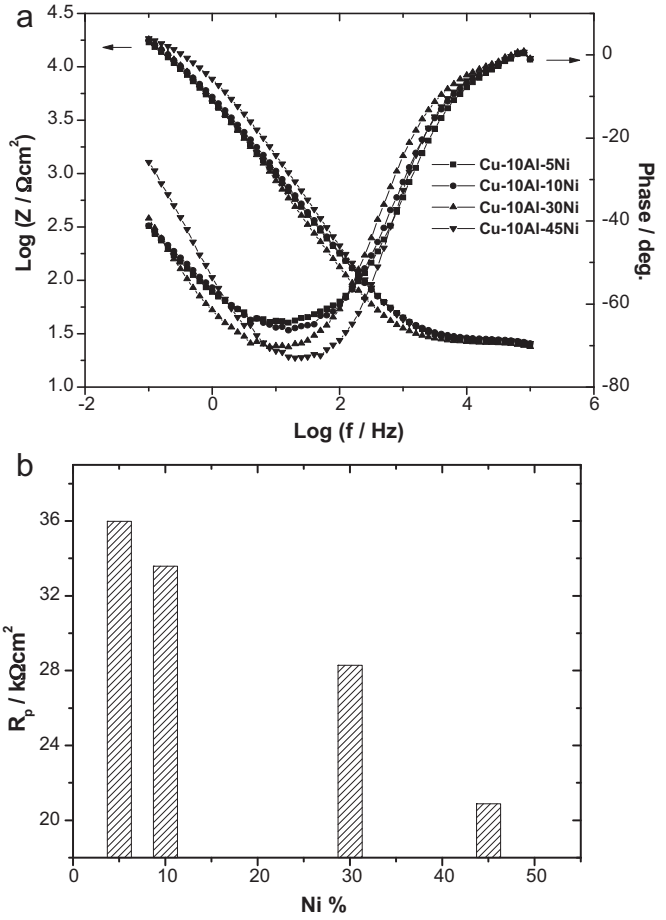

Fig. 8. (a) Bode plots for Cu–Al–Ni alloys in chloride free naturally aerated aqueous solutions of pH 7.0 at 25 °C. (b) Variation of the corrosion resistance of the Cu–Al–Ni alloys in chloride free naturally aerated aqueous solutions of pH 7.0 at 25 °C as a function of the Ni content.

Table 4
Equivalent circuit parameters for the different Cu–Al– Ni alloys after 1h of alloy immersion in chloride free naturally aerated neutral solutions, at 25 °C.

Alloys	R_s/Ω	$R_p/k\Omega\,cm^2$	$C_{dl}/\mu F\,cm^{-2}$	α
Cu–Al–5Ni	5.3	36.0	35.4	0.99
Cu–Al–10Ni	3.8	33.7	29.9	0.99
Cu–Al–30Ni	8.8	28.3	35.6	0.99
Cu–Al–45Ni	8.5	21.0	24.1	0.99

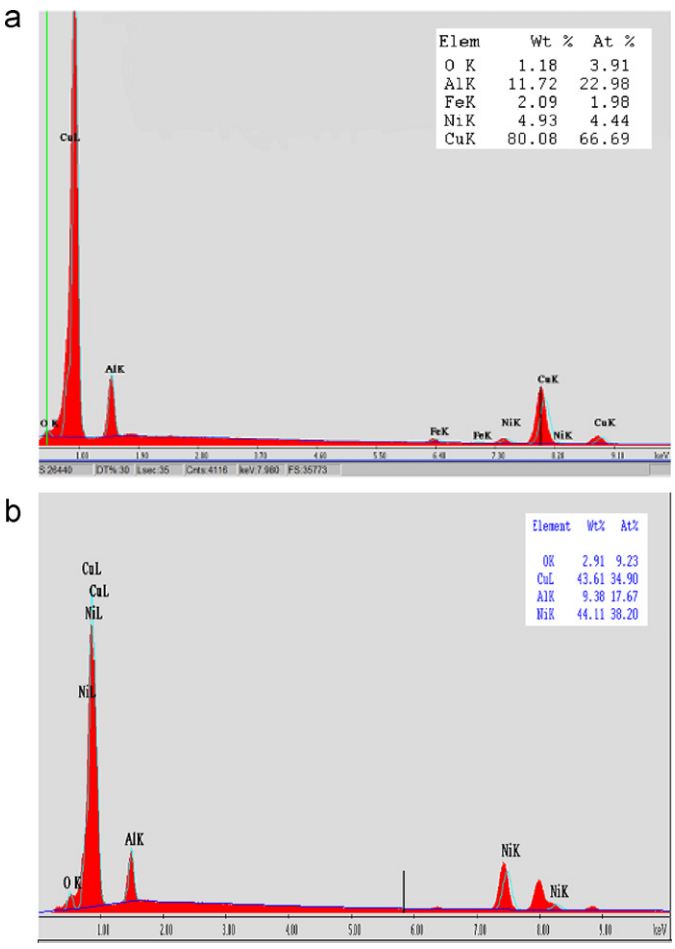

Fig. 9. (a) EDX analysis of the Cu–Al–5Ni alloy after 5 h immersion in chloride free naturally aerated aqueous solutions of pH 7.0 at 25 °C. (b) EDX analysis of the Cu–Al–45Ni alloy after 5 h immersion in chloride free naturally aerated aqueous solutions of pH 7.0 at 25 °C.

The higher corrosion resistance of the alloys compared to copper was related to the improved electronic structure due to incorporation of nickel ions into the crystal lattice of the Cu_2O inner layer [9]. In the point defect model (PDM) [32] and the solute vacancy interaction model (SVIM) [33], the Cu_2O film is regarded as a p-type semiconductor, and therefore the mobile cation vacancies $(V_{Cu}-(ox)_{red}$ are the main charge carriers (cf. Eq. (14). Ni from the alloy segregates into the Cu_2O barrier layer via a solid-state reaction where Ni^{2+} cations interact with mobile negatively charged cation vacancies and form neutral complexes according to [34]:

$$Cu_{Cu}(ox) \rightarrow Cu^{+}(aq) + V_{Cu}-(ox), \quad (14)$$

$$Ni_{Ni}(m) + 2\,V_{Cu}-(oX) \rightarrow [Ni_{Cu}(V_{Cu})_2] + 2e^{-} \quad (15)$$

The complex formation leads to a decrease of ionic and increase of electronic conductivity of the barrier layer, resulting in an increased corrosion resistance of the alloy surface film. Because the surface layer on the Cu–Al–Ni alloy with low Ni content shows the highest barrier properties, it can be concluded that the annihilation of oxide defects with Ni^{2+} ions occurs according to Eq. (15).

3.5. Surface analysis

The morphology of the alloy surfaces was investigated before and after 5 h immersion in the chloride free neutral solutions. It turned out that the alloy with high nickel content (45%) possesses rougher surface with more pits than the alloy with low nickel content (5%). The surface was analyzed by EDX. The EDX analysis for Cu–10Al–5Ni and Cu–10Al–45Ni alloys is presented in Fig. 9a and b, respectively. The data of surface analysis are also included. It is clear from the surface analysis data that the alloy with the low Ni content is Cu and Al rich on the surface, which leads to surface passivation and lower corrosion rate. Alloys with higher Ni content have nickel rich surface which decrease the corrosion resistance of the alloy as was confirmed by both the potentiodynamic and EIS measurements.

4. Conclusion

The corrosion rate of the Cu–Al–Ni alloys in chloride free neutral solutions increases with increasing the nickel content. Long immersion of the alloys in the electrolyte improves the corrosion resistance due to the formation of a thick adherent protective film. The passive film formation under different condition proceeds via a dissolution/precipitation mechanism. As the oxide film thickness increases the corrosion resistance increases leading to a decrease in the corrosion rate. The compact and protective film has a negligible effect on the cathodic process, but reduces the anodic dissolution rates. Alloys with high Ni content have Ni rich surfaces which lead to lower corrosion resistance.

References

[1] G. Kear, B.D. Barker, F.C. Walsh, Corros. Sci. 46 (2004) 109.
[2] A.H. Tuthill, Mater. Perform. 26 (1987) 12.
[3] G. Kear, B.D. Barker, K. Stokes, F.C. Walsh, J. Appl. Electrochem. 34 (2004) 659.
[4] M.G. Fontana, Corrosion Engineering, third ed., McGraw-Hill Inc., New York, 1986, p. 240.
[5] C. Kato, J.E. Castle, B.G. Ateya, H.W. Pickering, J. Electrochem. Soc. 127 (1980) 1897.
[6] C. Kato, H.W. Pickering, J. Electrochem. Soc. 131 (1984) 1219.
[7] J. Mathiyarasu, N. Palaniswamy, S. Muralidharan, Proc. Indian Acad. Sci. (Chem. Sci.) 113 (2001) 63.
[8] M. Urquidi-Macdonald, D.D. Macdonald, J. Electrochem. Soc. 136 (1989) 961.
[9] R.F. North, M.J. Pryor, Corros. Sci. 10 (1970) 297.
[10] G. Kear, B.D. Barker, K.R. Stokes, F.C. Walsh, J. Appl. Electrochem. 34 (2004), 1235, 1241.
[11] A. Schussler, H.E. Exner, Corros. Sci. 34 (1993) 1803.
[12] W.A. Badawy, K.M. Ismaila, A.M. Fathi, Electrochim. Acta 50 (2005) 3603.
[13] W.A. Badawy, F.M. Al-Kharafi, A.S. El-Azab, Corros. Sci. 41 (1999) 709.
[14] R.M. El-Sherif, K.M. Ismail, W.A. Badawy, Electrochim. Acta 49 (2004) 5139.
[15] W.A. Badawy, N.H. Hilal, M. El-Rabiee, H. Nady, Electrochim. Acta 55 (2010) 1880.
[16] K.M. Ismail, A.M. Fathi, W.A. Badawy, Corros. Sci. 60 (2004) 795.
[17] A. Jardy, A. Legal Lasalle-Molin, M. Keddam, H. Takenouti, Electrochim. Acta 37 (1992) 2195.
[18] J.C. Scully, The Fundamentals of Corrosion, Pergamon Press, Oxford, 1990.
[19] K.M. Ismail, W.A. Badawy, J. Appl. Electrochem. 30 (2000) 1303.
[20] H.H. Strehblow, B. Titze, Electrochem. Acta 25 (1980) 839.
[21] H.C. Man, D.R. Gabe, Corros. Sci. 21 (1981) 323.
[22] F.M. Al-kharafi, W.A. Badawy, Electochim. Acta 42 (1997) 579.
[23] W.A. Badawy, F.M. Al-Kharafi, A.S. El-Azab, Curr. Top. Electrochem. 6 (1998) 149.
[24] J.A. Wharton, R.C. Barik, G. Kear, R.J.K. Wood, K.R. Stokes, F.C. Walsh, Corros. Sci. 47 (2005) 3336.
[25] M. Pourbaix, Atlas of Electrochemical Equilibrium Diagrams in Aqueous Solutions, NACE, Houston, TX, 1966.
[26] A. Roine. Outokumpu HSC chemistry for windows (Version 4.0), Outokumpu Research Oy, Pori, Finland, 2000.
[27] I. Milosev, M.H. Metikos, Electrochim. Acta 42 (1997) 1537.
[28] R.G. Blundy, M.J. Pryor, Corros. Sci. 12 (1972) 65.
[29] K.M. Ismail, A.M. Fathi, W.A. Badawy, J. Appl. Electrochem. 34 (2004) 823.
[30] K. Hladky, L.M. Calow, J.L. Dawson, Br. Corros. J. 15 (1980) 20.
[31] J. Hitzig, J. Titz, K. Juettner, W.J. Lorenz, E. Schmidt, Electrochim. Acta 29 (1984) 287.
[32] D.D. Macdonald, J. Electrochem. Soc. 139 (1992) 3434.
[33] D.D. Macdonad, M. Urquidi, J. Electrochem. Soc. 132 (1985) 555.
[34] H. Shih, H.W. Pickering, J. Electrochem. Soc. 134 (1987) 1949.